Journal of Materials Chemistry B

Accepted Manuscript

ROYAL SOCIETY OF CHEMISTRY

www.rsc.org/materialsB

Drug loaded phosphate glass/hydroxyapatite nanocomposite for orthopedic applications

Raji Govindan, Easwaradas Kreedapathy Girija*

Department of Physics, Periyar University, Salem 636 011, Tamilnadu, India

*Corresponding author:Tel: +91 9444391733, Fax: +91 427 2345124.
E-mail: girijaeaswaradas@gmail.com (Easwaradas Kreedapathy Girija)

Abstract:

In orthopedic surgery, bone infection (osteomyelitis) is one of the most challenging issues encountered in the last few decades and the local drug delivery is the key strategy to overcome this issue. Drug loaded bioactive hydroxyapatite based nanocomposite bone substitutes are widely studied materials for local drug delivery application. In the present work, cylindrical shaped gentamicin sulfate (GS) loaded phosphate glass/hydroxyapatite (PG/HA) nanocomposite has been developed. The physico-chemical characterization and *in vitro* bioactivity and biocompatibility of the synthesized PG/HA nanocomposite were studied. Dissolution studies demonstrated that PG/HA nanocomposite has better degradation than pristine PG and HA. Drug loaded PG/HA nanocomposite exhibited higher antibacterial activity against *Staphylococcus aureus (S. aureus*) and *Escherichia coli (E. coli).* Also the nanocomposite displayed good apatite forming ability in simulated body fluid, a sustained drug release profile and excellent cytocompatibility with MG63 cells. The developed PG/HA nanocomposite can be a promising carrier for drug delivery in treating osteomyelitis.

1. Introduction

Annually millions are in need of bone repair procedures for bone defects caused by disease, trauma or habitual defects. In particular, osteomyelitis caused by bacteria such as *S. aureus* and *E. coli* remains one of the most challenging problems in the field of bone regeneration and systematic clinical antibiotic treatment needs 4-6 weeks.[1] Local drug delivery is considered to be a successful approach for the treatment of osteomyelitis[2] and drug loaded implants are highly preferred. Commercial poly(methyl methacrylate) (PMMA) has been used as a drug carrier for curing many types of bone tissue infection for several decades, however, PMMA is bioinert, so an additional operation is needed for its removal, which is expensive and painful.[3] Poly(lactic-co-glycolic) acid (PLGA) is biodegradable and widely used as a carrier material for controlled drug release, but the acidic environment resulting from its degradation can be harmful to a healthy bone tissue.[4] Biopolymers including chitosan (CH),[5] sodium alginate (SA)[6] and guar gum[7] have also been used for local drug delivery. However, weak mechanical properties and burst release of the drugs are major disadvantages, when pristine biopolymers are used as carriers. Ceramic/polymer nanocomposite drug carriers offer controlled and prolonged drug delivery at local sites and leads the reparative growth of the natural bone. [8-9]

Bioceramic carriers are fast becoming a replacement for polymers in local drug delivery as far as orthopedic applications are intended. Bioceramic entities such as calcium phosphate cement (CPC),[10] hydroxyapatite,[11-12] tricalcium phosphate,[13] and bioactive glass[14] have been used for tissue engineering and drug delivery. In particular bioglass (BG), nanocrystalline hydroxyapatite (n-HA) and their composites have been developed over the last decade for biomedical applications.[15] Synthetic n-HA is one of the most extensively investigated materials for biological applications including bone regeneration, tissue engineering, dental applications, local drug delivery *etc* because of its high surface activity, good biocompatibility, strong ability to adsorb a variety of chemical species and osteoconductivity *etc.*[16-18] However, the drawback is the weak interaction between the drug molecules and the n-HA particles often lead to an initial burst release of the drugs from the formed n-HA-drug interface.[19-20] Phosphate based glass ceramics possess enormous potential as biomaterials, due to their bone forming ability, tunable dissolution properties, antibiotic drug delivery and biocompatibility.[21-22] Enhanced dissolution and improved durability was found in presence of Fe_2O_3 in the glass network.[23] Sr^{2+} has

inhibited bone resorption and promotes bone formation, resulting in enhanced bone mass.[24-25] They are versatile materials for the fabrication of resorbable biomedical devices for orthopedic applications.

Gentamicin sulfate (GS) is extensively used as an antibiotic to prevent bone implant associated infection, due to its low cost, broad antibacterial spectrum of action, and good stability.[26] Gentamicin is one of the heat-stable antibiotics that remain active even after autoclaving. So, it is used during orthopedic surgery when high temperatures are required. Over 60% of chronic osteomyelitis cases were caused by *S. aureus* which is sensitive to gentamicin.[27]

In this present study, we assessed the *in vitro* dissolution, surface mineralization, cytocompatibility, drug release and antibacterial activity of cylindrical shaped GS loaded PG/HA nanocomposite for orthopedic applications.

2. Materials and methods

2.1 Media and chemicals

Calcium carbonate ($CaCO_3$, 99%) was purchased from Acros Organics (New Jersey, USA). Calcium nitrate tetrahydrate ($Ca(NO_3)_2{\cdot}4H_2O$, 98%), di-ammonium hydrogen phosphate ($(NH_4)_2HPO_4$, 99%), sodium chloride (NaCl, 99.5%), sodium hydrogen carbonate ($NaHCO_3$, 99.5%), potassium chloride (KCl, 99%), disodium hydrogen phosphate (Na_2HPO_4, 99%), magnesium chloride hexahydrate ($MgCl_2.6H_2O$, 99%), sodium sulfate (Na_2SO_4, 99.5%), TRIS buffer ($(CH_2OH)_3CNH_2$, 99.8%), calcium chloride dihydrate ($CaCl_2.2H_2O$, 99.5%), potassium dihydrogen phosphate (KH_2PO_4, 99.5%), HCl (Titrisol®), ammonium di-hydrogen phosphate ($NH_2H_2(PO_4)$, 99%), sodium carbonate ($NaCO_3$, 99%), ethylenediaminetetraacetic acid (EDTA, 99%) and strontium nitrate ($Sr(NO_3)$, 99%) were obtained from Merck chemicals (Mumbai, India). Iron oxide (Fe_2O_3) was obtained from Nice chemicals (Kochi, India). Gentamicin sulfate (GS), Muller Hinton broth and agar-agar nutrient were purchased from Hi-Media Laboratories Pvt Ltd (Mumbai, India).

2.2 Microorganisms and cell line

S. aureus (MTCC 96) and *E. coli* (MTCC 433) were used for antibacterial activity experiment, and they were procured from the Microbial Type Culture Collection (MTCC), Chandigarh, India,

and the human osteosarcoma cell line (MG-63) was obtained from National Centre for Cell Science (NCCS), Pune, India.

2.3 Preparation of hydroxyapatite (HA)

1M of calcium nitrate tetrahydrate and 0.6 M of di-ammonium hydrogen phosphate solution were prepared separately with molar ratio of Ca/P 1.67. The pH of both solutions were adjusted to 10 using ammonium hydroxide and ultrasonicated for 30 min. Di-ammonium hydrogen phosphate was added dropwise into calcium nitrate tetrahydrate solution under vigorous stirring for 30 min. The obtained precipitate was placed in microwave oven (LG, India) and irradiated with microwave at 900W, 2.45GHz, for 10 min. The suspension was centrifuged, filtered, washed and dried in hot air oven (Labline, India) at 80 °C for 24 h.[28]

2.4 Preparation of phosphate Glass (PG)

Phosphate glass $45P_2O_5$-24CaO-$16Na_2O$-5SrO-$5Fe_2O_3$ (mol.%), was synthesized by conventional melt quenching method. Calculated amounts of the precursors ($NH_4H_2(PO_4)$, $CaCO_3$, $NaCO_3$, $Sr(NO_3)$and Fe_2O_3) was weighed and ground using mortar and pestle for about 1 h. The obtained homogeneous mixture was preheated at 400 °C (NSW, New Delhi, India) for 1 h to eliminate CO_2, NH_3 and H_2O residuals. The homogenized mixture was melted in silica crucible at 1000 °C for 1 h, followed by quenching. The resulting glasses were ground and sieved to obtain fine glass powder.

2.5 Optimization of temperature and composition

In order to optimize the PG, HA composition and sintering temperature, samples PG, HA and PG/HA composites with PG & HA in the ratio 1:3, 2:2 and 3:1 named as PH31, PH22 and PH13 respectively were sintered at 600 °C and 1000 °C for 1 h and the product was analyzed by XRD and scanning electron microscopy (SEM). Based on the XRD and SEM results, the sintering temperature 600 ºC and composition PG:HA (1:3) [PH13] were chosen for further studies. As prepared HA will be referred as n-HA and PH13 sintered at 600 °C will be called as PG/HA nanocomposite hereafter.

2.6 Cylindrical shaped sample preparation

Cylindrical shaped PG, n-HA and PG/HA nanocomposite samples were prepared by mixing 100 mg of the powdered sample with de-ionized water and the slurry was then put into plastic syringe and allowed to harden at room temperature (RT) for 24 h. The hardened solid cylindrical shaped PG, n-HA and PG/HA nanocomposite samples were withdrawn from the plastic syringe. GS (Fig. 1) loaded cylindrical PG, n-HA and PG/HA nanocomposite samples were prepared by mixing appropriate amount of GS in the slurry and hardened as described above. Photograph of cylindrical shaped samples are shown in Fig. 2.

2.7 Characterization

Powder X-ray diffraction (XRD) patterns were recorded on a Rigaku MiniFlex II diffractometer (Tokyo, JAPAN) in the range $10^{o} \leq 2\theta \leq 60^{o}$ with Cu Kα radiation (1.5406 Å). The surface morphology of the composite samples sintered at different temperatures was analyzed by SEM (VEGA TESCAN, Brno, Czech Republic). Particle size analysis was performed at room temperature using dynamic light scattering (DLS; ZetaSizer NS, Malvern Instruments Ltd., Worcestershire, UK). The functional group identification of PG, n-HA and PG/HA nanocomposite was done by recording the FTIR spectra in a Perkin Elmer RXI FTIR spectrometer (Perkin Elmer, Massachusetts, USA) by KBr pellet technique in the wave number range from 4000 to 400 cm^{-1} at room temperature. The specific surface area of n-HA and PG/HA nanocomposite was determined by the N_2 Brunauer-Emmett-Teller (BET) nitrogen adsorption method in a Micromeritrics Gemini VII 2390 surface area analyzer. The samples were dried, degassed and analyzed using a multipoint N_2 adsorption/desorption method at room temperature.

2.8 Dissolution and apatite forming ability

Both the dissolution and apatite formation ability of the cylindrical shaped PG, n-HA and PG/HA nanocomposite samples were carried out in SBF solution. SBF had an ionic concentration (Na^{+} 142.0, K^{+} 5.0, Ca^{2+} 2.5, Mg^{2+} 1.5, Cl^{-} 125.0, HPO^{4-} 1.0, HCO_3^{2-} 27.0, SO_4^{2-} 0.5 mmol L^{-1}) nearly equivalent to that of human plasma,[29] with the starting pH of SBF solution 7.4. *In vitro* dissolution of PG, n-HA and PG/HA nanocomposite was measured from Ca^{2+} ion estimation by ethylenediaminetetraacetic acid (EDTA) titration technique.[30] The samples were

soaked in 25 mL of simulated body fluid (SBF; pH = 7.4) and incubated at 37 ± 0.5 °C for 3, 6, 9,12,15,18 and 21 days. After the incubation period, the sample soaked SBF solution was collected and calcium ion (Ca^{2+}) concentration was estimated. The sample soaked solution was taken into a conical flask and added 4 mL of 8 M sodium hydroxide solution then added small amount of Patton- Reeder indicator and swirled the solution to dissolve the indicator and finally titrated against 0.025 M of EDTA solution. The endpoint was a color change from pink/red to blue. The experiment was repeated three times to get average value and standard deviation. The concentration of calcium was determined using the following equation:

$$EDTA_{mol} \times V_{EDTA} = Ca^{2+}_{mol} \times V_{Ca^{2+}}$$

The variation in pH of the degradation medium (SBF solution) was measured everyday during the dissolution study for all the three samples.

To investigate the apatite forming ability, cylindrical shaped samples weighing 0.1 g were soaked in 30 mL of SBF solution in a polyethylene plastic container and were placed in an incubator at 37 °C (±0.5 °C) under static condition and the SBF solution was renewed every 3 days interval. After 21 days, the samples were collected from SBF solution, rinsed with ethanol and dried. SEM observation was used to check the apatite formation on the surfaces of cylindrical shaped samples.

2.9 Drug release

The pre weighed GS loaded PG, n-HA and PG/HA nanocomposite samples were immersed in 25 mL of PBS in polyethylene container and incubated in an orbital shaker at 37 °C at 100 rpm. 1 mL of aliquot was withdrawn and replaced by the same amount of fresh PBS for predetermined time. The extracted medium was diluted to a desired concentration with PBS and the concentration of GS was measured at 256 nm using UV-Vis spectrometer (Perkin Elmer). The experiments were repeated in triplicate to get mean and the standard deviation.

2.10 Drug release kinetics

The methods of approach used to investigate the kinetics of drug release formulations are Higuchi model and Ritger–Peppas model. Ritger–Peppas,[31] model is being represented by the following equation:

$$Q = kt^n$$

Higuchi developed models to study the release of water soluble and poor soluble drugs incorporated in semisolid and solid matrices.[32] This model is being represented by the following equation:

$$Q = kt$$

where Q is the fraction of drug released at time t, k is the rate constant and n is the release exponent which defines the mechanism of drug release. The value of n is determined from the slope of the plot of the logarithm of Q vs logarithm of time. This model is generally applicable upto 60% of total drug amount is released.

2.11 Antibacterial activity

The osteomyelitis causing gram-positive and gram-negative pathogens such as *S. aureus* and *E. coli* were used to test the antibacterial activity of the PG, n-HA and PG/HA nanocomposite samples. The six (without GS and with GS) cylindrical shaped samples were tested against bacterial strains by agar disc diffusion method. Pure culture was sub cultured in Muller Hinton (MH) broth for 24 h at 37 °C. Then, each strain was swabbed uniformly into the individual MH agar plates using sterile cotton swabs. The cylindrical shaped samples were placed on the agar plates and incubated at 37 °C for 24 h to measure the level of inhibition.

2.12 Cytocompatibility

The cytotoxicity test was done for PG, n-HA and PG/HA nanocomposite with the human osteosarcoma cell line (MG-63) grown in Eagles Minimum Essential Medium containing 10% fetal bovine serum (FBS) with 100 U mL^{-1} penicillin/streptomycin. The cells were maintained at 37 °C in 5% CO_2, 95% air and 100% relative humidity. Maintained cultures were passaged every week, and the culture medium was changed twice a week. The monolayer cells were detached with trypsin-ethylenediaminetetraacetic acid (EDTA) to make single cell suspensions and viable cells were counted using a hemocytometer and diluted with medium containing 5% FBS to give

final density of $1x10^5$ cells mL^{-1}. 100 µL per well of cell suspension were seeded into 96-well plates at plating density of 10,000 cells/well and incubated at 37 °C in 5% CO_2, 95% air and 100% relative humidity. After 24 h incubation, samples PG, n-HA and PG/HA nanocomposite were added to the culture medium at varying dosages 12.5, 25, 50, 100 and 200 µg mL^{-1}. Before adding, the samples were sterilized by immersing in 70% ethanol for 2 h and were then washed with PBS solution. Aliquots of 100 µl of these different sample dilutions were added to the appropriate wells already containing 100 µl of medium with or without cells (blank), resulting in the required final sample concentrations. The medium containing without PG, n-HA and PG/HA nanocomposite were served as positive control. The plates were further incubated for 48 h at 37 °C in 5% CO_2, 95% air and 100% relative humidity. The assay was performed in triplicate.

After 48 h of incubation, 15 µL of 3-[4,5-dimethylthiazol-2-yl]2,5-diphenyltetrazolium bromide (MTT) (5 mg mL^{-1}) in phosphate buffered saline (PBS) was added to each well and incubated at 37 °C for 4 h. The medium with MTT was then flicked off and the formazan crystals were solubilized in 100 µL of DMSO and measured the absorbance at 570 nm using micro plate reader. The percentage of cell viability was then calculated with respect to control as follows,

$$\% \text{ Cell viability} = [OD] \text{ Test} / [OD] \text{ Control} \times 100$$

3. Results and discussion

3.1 X-ray diffraction (XRD)

The XRD patterns of the as prepared samples PG, HA, PH13, PH22, PH31, and the sintered samples at temperatures viz., 600 °C and 1000 °C are shown in Fig. 3. The XRD pattern of as prepared PG powder reveals the amorphous nature of the sample (Fig. 3a). The XRD patterns of as prepared HA and PG/HA composite are in good agreement with the standard JCPDS data for HA (09−0432). This suggested that the as prepared sample contained no other phases except HA.

Table1 The crystalline parameters of HA powder.

Sample	Lattice parameter (Å)		D_{hkl} (nm)[a]	V (Å^3)[b]	c/a[c]
	a = b	c			
As prepared	9.4270	6.9070	24	531.560	0.7326
600 °C	9.4265	6.8599	25	527.882	0.7277

[a]Crystallite size.
[b]Unit cell volume.
[c]Lattice distortion

Heat treatment resulted in the formation of bioactive glass – ceramics in the samples containing PG. The samples sintered at 600 °C exhibited different phases like tromelite ($Ca_4P_6O_{19}$), β-calcium meta-phosphate [β-$Ca(PO_3)_2$] and α-calcium pyrophosphate (α-$Ca_2P_2O_7$) and the concentration of these phases are higher for the sample containing high glass content. The broad peaks suggest the existence of nano-sized crystals and the less crystalline nature of the sample. When the sintering temperature was increased to 1000 °C, phases like - tromelite, α-calcium pyrophosphate, β-tricalcium phosphate [β-TCP, $Ca_3(PO_4)_2$] and β-calcium meta-phosphate became the major components in the sintered product and their crystallinity was very high. The crystallite size of the as-synthesized and 600 °C heat treated samples was calculated from XRD data using the Debye–Scherrer approximation. The crystallite size and crystalline parameters of the as-synthesized and 600 °C heat treated samples are given in Table 1. It is evident that the crystallite size of the both as prepared and 600 °C sintered HA were 24 nm and 25 nm respectively. Whereas, the sample PH13 sintered at 600 °C is observed to retain more nano crystalline HA.

3.2 Particle size distribution

The particle size distribution of PG, n-HA and PG/HA nanocomposite samples measured by DLS analyzer are shown in Fig. 4. The histograms show that the mean particle size of the PG is 1755 ± 405.34 nm (i.e. around 2 μm). n-HA sample had an average particle size of about 240 ± 45.3 nm with size distribution from 190.1 to 295.3 nm and PG/HA nanocomposite is 327 ± 89.37 nm with approximate size range between 220 and 458.7 nm.

3.2 Specific surface area analysis

The drug-release kinetics could be controlled by specific surface area of the carrier, which makes them potent system for the storage and controlled release of drugs. The specific surface area of n-HA and PG/HA nanocomposite samples were measured by the N_2 adsorption/desorption isotherms at relative pressure (P/P_0) between 0.0 and 0.3. The Brunauer-Emmett-Teller (BET) specific surface area of n-HA and PG/HA nanocomposite were 46.39 m^2g^{-1} and 22.33 m^2g^{-1}, respectively. These results indicated that specific surface area changes occurred when making composite with PG and n-HA sample.

3.4 FT-IR analysis

The FT-IR spectra of PG, n-HA and PG/HA nanocomposite are shown in the Fig. 5.The bands at 540 cm^{-1}, 751 cm^{-1}, 903 cm^{-1} and 1109 cm^{-1} were attributed to the symmetric (ν_1) stretching vibration of PO_3^{2-} of phosphate group in PG sample. The PO_2 asymmetric (ν_2) characteristic vibration is observed at 1275 cm^{-1}. A structure of n-HA is characterized by different vibrational modes of the phosphate PO_4^{3-} and hydroxyl OH^- groups. The characteristic PO_4^{3-} (ν_4) vibrations of HA appeared at 569 and 615 cm^{-1} along with other phosphate peaks at 446 cm^{-1} (ν_1), 980 cm^{-1} (ν_2), 1042 cm^{-1} (ν_3). The band at 3574 cm^{-1} is the characteristic O–H stretching mode of n-HA.[33] The peaks corresponding to the water molecules associated with HA are seen at 3442 cm^{-1} and 1635 cm^{-1}. The bands observed in 1426 cm^{-1} corresponds to carbonate impurities and such carbonation was due to the reactive absorption of atmospheric carbon dioxide by the samples during the sample preparation.[34] However, when sintered at 600 °C, in addition to the peaks of n-HA and PG the PO_3^- (ν_2) vibrational band of $Ca_4P_6O_{19}$ phase was observed at 1175 cm^{-1}.[35]

3.5 Morphological investigations

Fig. 6 shows the morphology of the samples PH31, PH22 and PH13 sintered at 600 °C and 1000 °C as observed in SEM. On 600 °C heat treatment, β-calcium meta-phosphate and α-calcium pyrophosphate phases evolved and as the content of PG increases these phases dominates and form a glassy matrix. The PH13 sample due to the less glass content exhibits more nano crystalline HA and nanoporosity. In the other samples PH22 & PH31 the nano HA is embedded in glassy matrix with less porosity. On the other hand 1000 °C heat treated sample PH13 showed distinct well faceted large crystals. But in the increased glass content samples the crystals were found to be present in the glass matrix.

3.6 Dissolution studies

The profile of *in vitro* calcium (Ca^{2+}) ion release from n-HA, PG and PG/HA nanocomposite samples at 3 days interval for 21 days is shown in Fig. 7a. The concentration of Ca^{2+} increased rapidly in all the three samples upto day 3 between 7-9 mM, followed by a gradual increase at day 21. The data points are average of at least three experiments.

The Ca^{2+} concentration reached 15.5, 13.9 and 12.3 mM for PG/HA nanocomposite, PG and n-HA respectively. The result shows that the PG/HA nanocomposite sample have better dissolution rate than the other two samples. The Ca^{2+} concentration depends on the formation of apatite on the sample.[36]

The pH variation of the SBF media during dissolution study is shown in Fig. 7b. pH measurement reveals a constant variation with cyclic increase and decrease pattern. The initial reduction of pH mainly depends on presence of Fe_2O_3 in the PG. Dissolution of n-HA releases OH^- ions into the medium that leads to the rise in pH in the initial days later the deposition of apatite consumes OH^- ions leading to the reduction in pH. But in the case of nanocomposite pH lies above 7.4 for the first 13 days then it is comes down below 7.4 in the rest of the experiment. The variation of pH can be correlated to the dissolution of ionic species from PG and n-HA samples in the soaking solution.[37]

3.7 GS drug release from samples

Fig. 8 shows the cumulative drug release profile for the three samples in PBS medium. All the three carriers exhibited an initial burst release for the first 5 h releasing almost 40-45% of the total drug loaded which is due to the dissolution of loosely attached GS molecules in the sample. The burst release was followed by a sustained release composed of two obvious stages and in the first stage about 80-90% of the drug was released in the order of n-HA<PG/HA<PG. Then the release became very minimum in the case of n-HA and nanocomposite, but glass showed almost complete drug release. Release of GS continued from n-HA and was close to 100% at 264 h but in the case of PG/HA nanocomposite release of the drug seemed to be terminated. Retention of a small amount of GS inside the nanocomposite sample may be due to the hydrogen bonding between P-OH group in PG/HA nanocomposite, and the hydroxyl and amino groups in the GS molecule.[38] The rapid delivery of drug during the initial burst release is required immediately after surgery for the effective inhibition of microorganisms and then a controlled release is needed to aid long-term healing and to avoid the toxic and adverse systemic effects caused by high concentration of antibiotics administrated orally. Further tuning of the PG/HA nanocomposite properties is needed for achieving the complete release of the drug from the matrix.

Table 2 Ritger–Peppas kinetic model parameters for GS release from three samples.
n: kinetic exponent, R^2: regression coefficient

Sample codes	*n*	R^2
PG	0.24	0.9219
n-HA	0.17	0.95144
PG/HA nanocomposite	0.23	0.9885

The sustained GS release from the carrier is associated with the diffusion mechanism hence the data were fitted to Ritger-Peppas and Higuchi models to establish the kinetics and release mechanisms. The fitting plots are shown in Fig. 9a-b and the n values are given in table 2. The GS release data for PG/HA nanocomposite (R^2: 0.9630) shows best fit with Higuchi model (Fig. 9a) among the samples. In order to confirm the diffusion mechanism, the GS release data were fitted into Ritger-Peppas model, which showed good linearity (R^2: 0.9885) for PG/HA nanocomposite sample, and is in good linear fit than for PG and n-HA samples, also it suggests that the value of *n* (Ritger–Peppas model) for the three samples are lower than 0.45 and the mechanism of GS release from all the samples followed Fickian diffusion (i.e. controlled release). Among the three samples PG/HA nanocomposite is found to be a better carrier.

3.8 Antibacterial activity

Fig. 10 shows the antibacterial effect of all the GS loaded and unloaded samples (control) against *S. aureus* and *E. coli*. The GS loaded samples showed clear zone of inhibition around the disc indicating the bacterial inhibition and the diameter of inhibition zone is given in table 3 which differs for different samples and organisms. An interesting observation made from this study is that a small zone of inhibition was observed around the unloaded PG sample for *E. coli* but not for *S. aureus*. This antibacterial effect of the PG specimen can be explained in terms of the glass composition, the glass dissolution rate, and the pH changes of the medium.[39-40] However, there is no inhibition in other two control samples, which revealed that GS antibiotic has good activity against *S. aureus* and *E. coli.* GS irreversibly binds the 30S subunit of the bacterial ribosome, interrupts protein synthesis and inhibits bacterial growth. The above study showed the antibacterial activity of GS loaded PG/HA nanocomposite is found to be better than PG and n-HA samples. The dissolution rate of nanocomposite is higher than the other two pristine samples which might be the reason for the enhanced antibacterial ability of it. In particular, GS is

more effective against Gram negative bacteria, so the zone of inhibition were larger for *E. coli* than *S. aureus*.

Table 3 Antibacterial activity of GS loaded PG, n-HA and PG/HA samples towards *S. aureus* and *E. coli.*

Samples	Diameter of zone of inhibition (mm)	
	S. aureus	***E. coli***
PG	29.6 ± 0.50	30.8 ± 0.25
n-HA	28.53 ± 0.53	30.76 ± 0.87
PG/HA nanocomposite	31 ± 0.40	32.93 ± 0.11

3.9 Bioactivity

Fig. 11 shows the SEM images of samples after soaking in SBF for 21 days. The SEM micrographs showed apatite deposition on the surface of the samples that was more prominent in the PG sample than for n-HA and PG/HA nanocomposite samples. But the apatite rich layer deposition on the surface of nanocomposite sample was better than on the n-HA sample, which is due to poor resorption of the n-HA sample. The rich apatite deposition on the surface of the PG sample is due to the Ca^{2+} and PO_4^{2-} ions leached from PG sample, that increased the degree of supersaturation of the surrounding SBF with respect to apatite thereby accelerating the apatite formation on the surface. Higher biodegradability of the α–$Ca_2P_2O_7$ component present in the PG/HA nanocomposite, enhanced its apatite formation better than for n-HA. These results indicate that, incorporation of glass in the n-HA shows better bioactivity than pure n-HA. The apatite forming ability strongly depends on the pH variation and dissolution of Ca^{2+} and PO_4^{2-} ions.[41-42]

3.10 Cytocompatibility

The material prepared is anticipated for biomedical applications hence, it is essential to measure cytocompatibility of the material. PG, n-HA and PG/HA nanocomposite samples were subjected for cytocompatibility study for different dosages and the result obtained are given in Fig. 12. PG, n-HA and PG/HA nanocomposite samples showed good cell viability since calcium phosphate is the main inorganic content of bone tissues. Cytocompatibility was found to decrease with increasing dosage of the sample. Optical image of osteoblast MG-63 cells and cells contained different dosages of PG/HA nanocomposite for 48 h incubation is shown in Fig. 13. According

to biological evaluation of medical devices - Part 5: Tests for *in vitro* cytocompatibility (ISO 10993 - 5: 2009), if cell viability of material is less than 70 % then it has a cytotoxic potential. However PG, n-HA and PG/HA nanocomposite samples exhibits cell viability greater than 70 % (Fig.12) demonstrating that the all samples are biocompatible with human osteoblast MG-63 cells.

4. Conclusions

In the present study, cylindrical shaped GS loaded PG, n-HA and PG/HA nanocomposite samples were successfully developed for orthopedic applications. The PG/HA nanocomposite was found to have better degradation, bioactivity, biocompatibility, and sustained and prolonged GS release than n-HA and PG samples. The Ridger-peppes model indicates GS release from PG/HA nanocomposite was Fickian diffusion. The result of antibacterial activity against *S. aureus* and *E. coli* revealed that GS loaded nanocomposite sample exhibited better zone of inhibition than the pristine samples. The apatite formation ability and cell viability were excellent for all the three samples. The present investigation has demonstrated that PG/HA nanocomposite could be used as a carrier for GS not only to eradicate the osteomyelitis caused by Gram-negative and Gram-positive bacteria, but also to repair the bone defect caused by the infection due to the tunable nanocomposite degradation.

Acknowledgments

This work was financially supported by University Grants Commission (UGC), India through project (Project Ref. No.: 41)1013/2012 SR). The discussions with Dr. A. Thamizhavel, Tata Institute of Fundamental Research are gratefully acknowledged. The authors are also thankful to Dr. P. Thilakan, Pondicherry University for his valuable help in BET analysis.

References

1. C. G. Lee, Y. C. Fu and C. H. Wang, *Biotechnol. Bioeng.,* 2005, **9**, 622–635.
2. S. K. Nandi, P. Mukherjee, S. Roy, B. Kundu, D. K. De and D. Basu, *Mater. Sci. Eng. C*., 2009, **29**, 2478–85.
3. S. Rossi, A. O. Azghani and A. Omri, *J. Antimicrob. Chemoth*., 2004, **54**, 1013–1018.
4. H. Liu, E. B. Slamovich and T. J. Webster, *Int. J. Nanomed.,* 2006, **1**, 541–545.

5. A. Bhat, M. Dreifke, C. Gomez, Y. Kandimalla, N. A. Ebraheim and A. C. Jayasuriya, *J. Tissue Eng. Regen. Med*., 2010, **4**, 532–542.

6. T. Hou, J. Xu, Q. Li, J. Feng and L. Zen, *Osteoarthr. Cartilage,* 2009, **17**, 1377–1384.

7. U. S. Toti and T. M. Aminabhavi, *J. Control. Release*. 2004, **95**, 567–77.

8. F. Sun, H. Zhou and J. Lee, *Acta Biomater.,* 2011, **7**, 3813–3828.

9. V. Uskokovic and T. A. Desai, *J. Pharm. Sci*., 2014, **103**, 567–579.

10. M. Ginebra, C. Canal, M. Espanol, D. Pastorino and E. B. Montufar, *Adv. Drug Deliv. Rev.,* 2012, **64**, 1090-1110.

11. Y. J. Guo, Y. Y. Wang, T. Chen, Y. T. Wei, L. F. Chu and Y. P. Guo, *Mater. Sci. Eng. C*., 2013, **33**, 3166-3172.

12. M. A. Rauschmann, T. A. Wichelhaus, V. Stirnal, E. Dingeldein, L. Zichner, R. Schnettler and A. Volker, *Biomaterials*, 2005, **26**, 2677–2684.

13. B Kundu, S. K. Nandi, S. Roy, N. Dandapat, C. Soundrapandian, S. Datta, P. Mukherjee, P. K. Mandal, S. Dasgupta and D. Basu, *Ceram. Int*., 2012, **38**, 1533-1548.

14. L. L. Hench and J. M. Polak, *Science*, 2002, **295**, 1014–1017.

15. R. Ravarian, F. Moztarzadeh, M. Solati Hashjin, S. M. Rabiee, P. Khoshakhlagh and M. Tahriri, *Ceram. Int*., 2010, **36**, 291-297.

16. G. S. Kumar and E. K. Girija, *Ceram. Int.,* 2013, **39**, 8293-8299.

17. G. Suresh Kumar, A. Thamizhavel and E.K. Girija, *Mater. Lett.,* 2012, **76**, 198-200.

18. R. Vani, S. B. Raja, T. S. Sridevi, K. Savithri, S. N. Devaraj, E. K. Girija, A. Thamizhavel and S. N. Kalkura, *Nanotechnology,* 2011, **22**, 285701.

19. M. Y. Ma, Y. J. Zhu, L. Li and S. W. Cao, *J. Mater. Chem*., 2008,**18**, 2722-7.

20. Y. R. Cai and R. K. Tang, *J. Mater. Chem*., 2008, **18**, 3775-87.

21. H. W. Kim, E. J. Lee, I. K. Jun, H. E. Kim and J. C. Knowles, *J. Biomed. Mater. Res. B Appl. Biomater*., 2005, **75**, 34-41.

22. E. A. Abou Neel, D. M. Pickup, S. P. Valappil, R. J. Newport and J. C. Knowles, *J. Mater. Chem*., 2009, **19**, 690–701.

23. I. Ahmed, C. A. Collins, M. P. Lewis, I. Oslen and J. C. Knowles, *Biomaterials*, 2004, **25**, 3223–3232.

24. E. Gentleman, Y. C. Fredholm, G. Jell, N. Lotfibakhshaiesh, M.D. O'Donnell, R.G. Hill and M. M. Stevens, *Biomaterials,* 2010, **31**, 3949–3956.

25. M. D. O'Donnell, P. L. Candarlioglu, C. A. Miller, E. Gentleman and M. M. Stevens, *J. Mater. Chem.,* 2010, **20**, 8934–8941.

26. M. R. Virto, P. Frutos, S. Torrado and G. Frutos, *Biomaterials,* 2003, **24**, 79–87.

27. J. M. Andrews, *J. Antimicrob. Chemoth*., 2001, **48**, 5-16.

28. N. Iqbal, M. R. Abdul Kadir, A. N. Nik Nik Malek, N. H. Mahmood, M. R. Murali and T. Kamarul, *Mater. Lett*., 2012, 89:118–122.

29. A. C. Tas, *Biomaterials,* 2000, **21**, 1429–1438.

30. G. S. Kumar, A. Thamizhave, Y. Yokogawa, S.N. Kalkura and E. K. Girija, *Mater. Chem. Phys*., 2012, **134**, 1127-1135.

31. P. L. Ritger and N. A. Peppas, *J. Control. Release*, 1987, **5**, 37–42.

32. T, Higuchi, *J. Pharm. Sci*. 1963, **52**, 1145-1149.

33. R. Karunamoorthi, G. Suresh Kumar, A. I. Prasad, R. K. Vatsa, A. Thamizhavel and E. K. Girija, *J. Am. Ceram. Soc*., 2013, **96**, 1-8.

34. M. N. Salimi, R. H. Bridson, L. M. Grover and G. A. Leeke, *Powder Technol.,* 2012, **218**, 109–18.

35. H. A. Höppe, *Z. Anorg. Allg. Chem.,* 2005, **631**, 127-1276.

36. A. Martínez, I. Izquierdo-Barba and M. Vallet-Regí, *Chem. Mater.,* 2000, **12**, 3080–3088.

37. A. G. Dias, M. A. Lopes, I. R. Gibson and J. D. Santos, *J. Non-Cryst. Solids*, 2003, **330**, 81-89.

38. M. Zhu, J. Zhang, C. Tao, X. He and Y. Zhu, *Mater. Lett*., 2014, **115**, 194-197.

39. D. M. Pickup, S. P. Valappil, R. M. Moss, H. L. Twyman, P. Guerry, M. E. Smith, M. Wilson, J. C. Knowles and R. J. Newport, *J. Mater. Sci*., 2009, **44**, 1858-1867.

40. S. P. Valappil, D. Ready, E. A. Abou Neel, D. M. Pickup, W. Chrzanowski, L. A. O'Dell, R. J. Newport, M. E. Smith, M. Wilson and J. C. Knowles, *Adv. Funct. Mater*., 2008, **18**, 732-741.

41. T. Kokubo, H. Kushitani, S. Sakka, T. Kitsugi and T. Yamamuro, *J. Biomed. Mater. Res.* 1990, **24**, 9-13.

42. D. K. Pattanayak, S. Yamaguchi, T. Matsushita, T. Nakamura and T. Kokubo, *J. R. Soc. Interface,* 2012, **9**, 2145-2155.

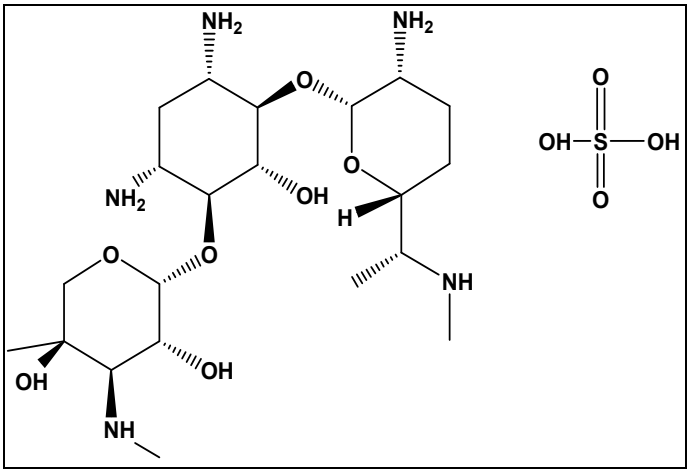

Fig. 1 Chemical structure of gentamicin sulfate drug molecule.

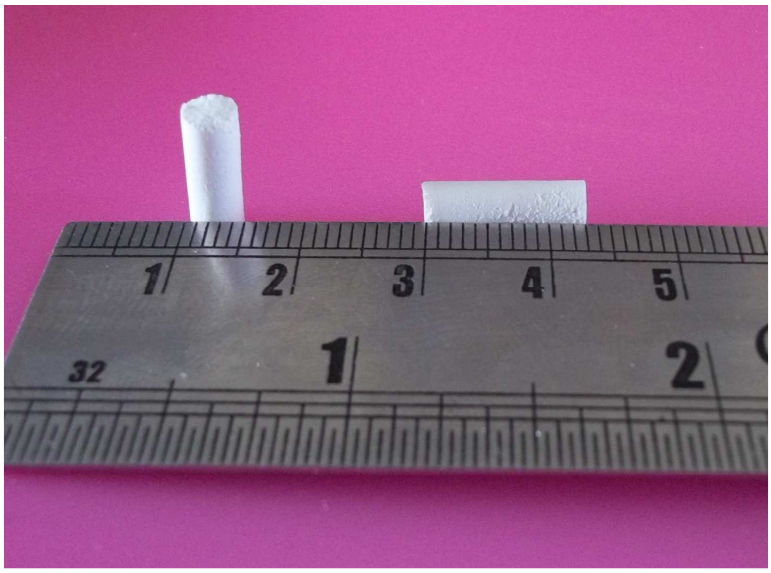

Fig. 2 Photograph of cylindrical shaped samples.

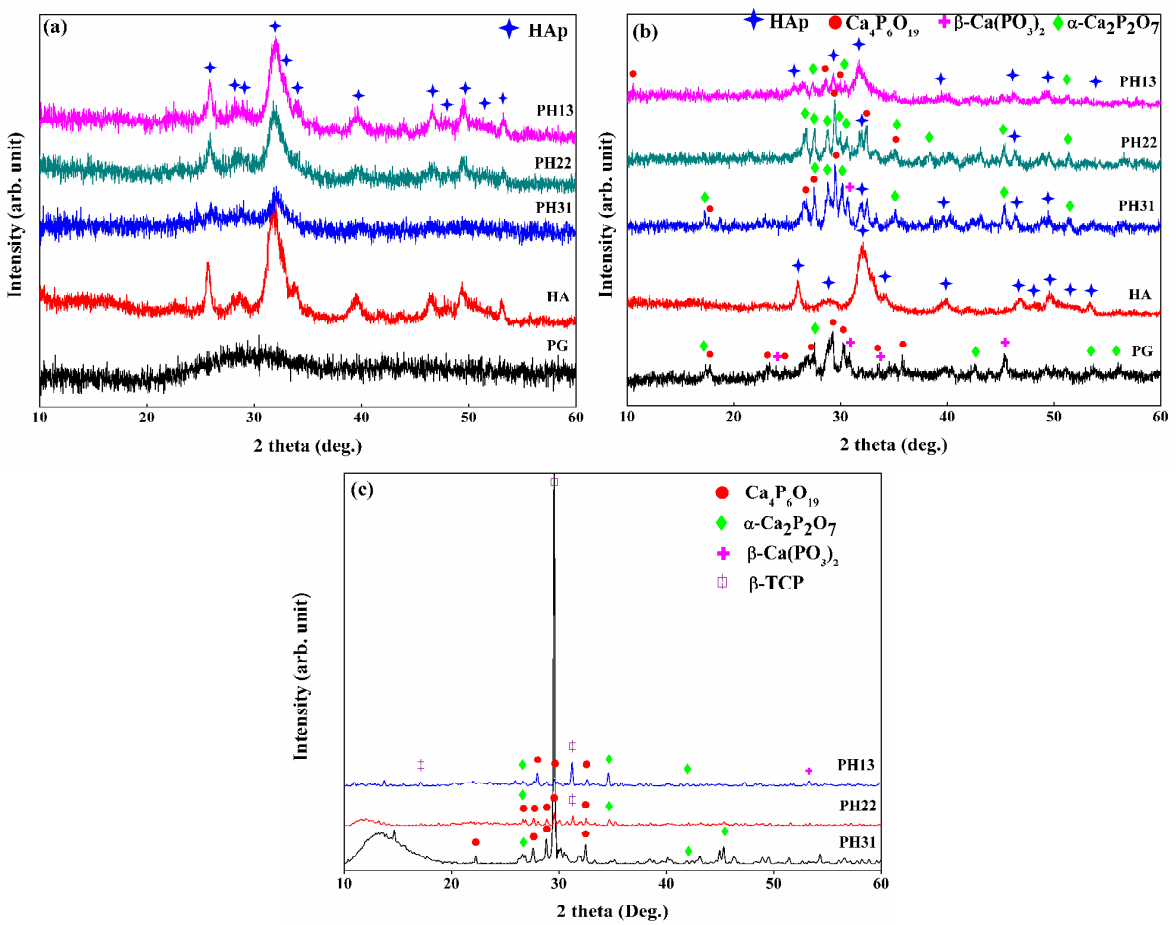

Fig. 3 XRD patterns of (a) as-prepared, sintered at (b) 600 °C and (c) 1000 °C.

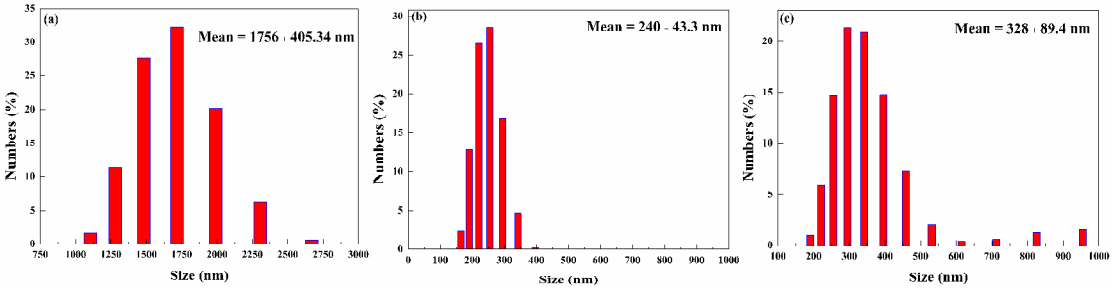

Fig. 4 Particle size of (a) PG, (b) n-HA and (c) PG/HA nanocomposite.

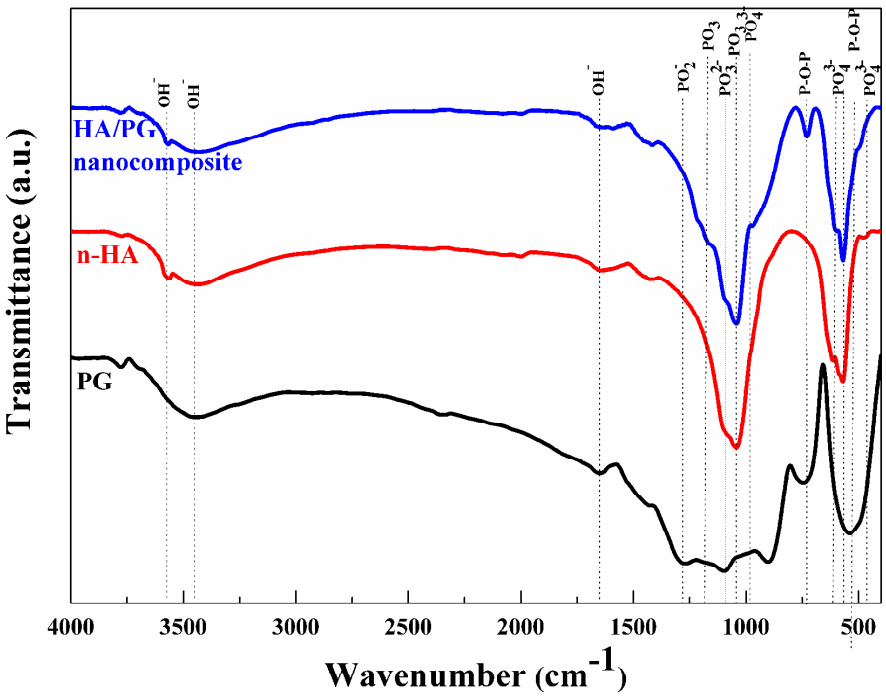

Fig. 5 FTIR spectra of PG, n-HA and PG/HA nanocomposite.

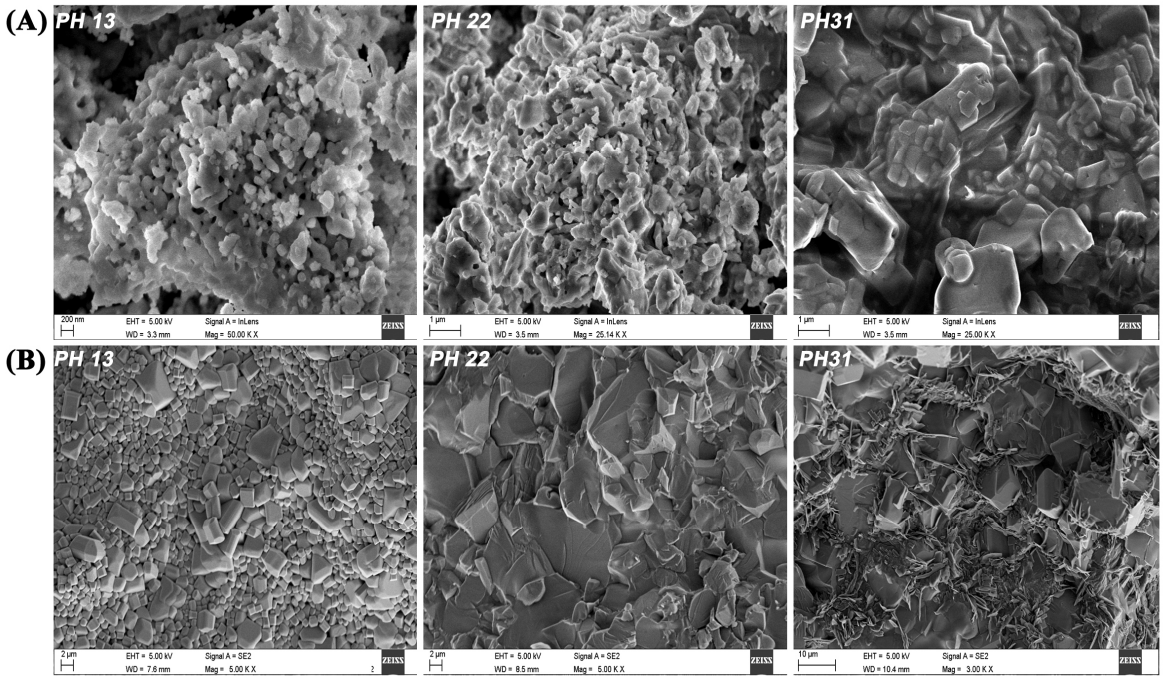

Fig. 6 SEM images of nanocomposite samples sintered at (A) 600 °C and (B) 1000 °C.

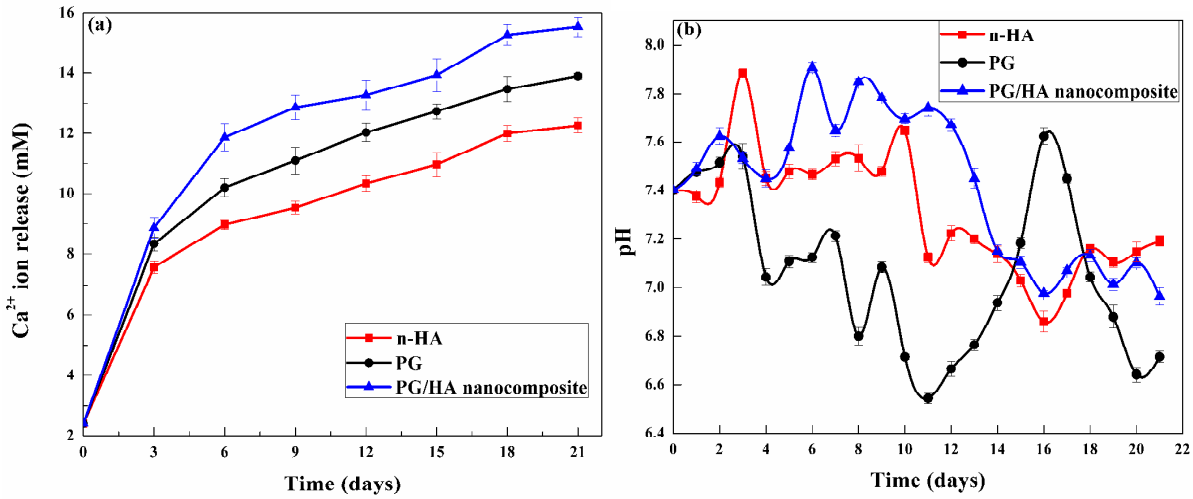

Fig. 7 Dissolution study of PG, n-HA and PG/HA nanocomposite samples after soaking in SBF, (a) calcium ion release and (b) pH variations.

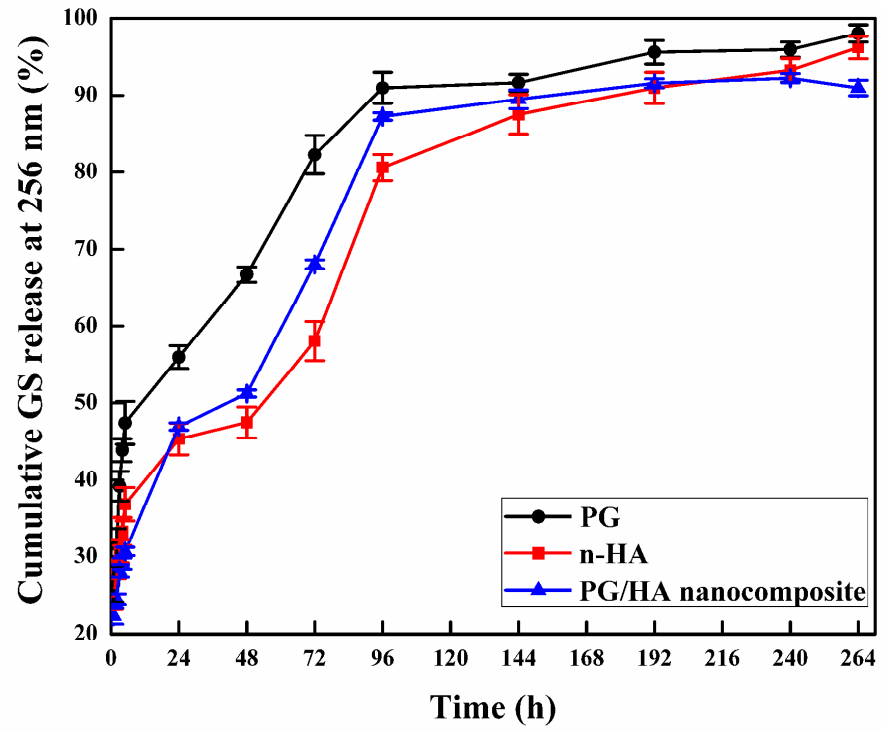

Fig. 8 *In vitro* cumulative GS release from the PG, n-HA and PG/HA nanocomposite samples against time.

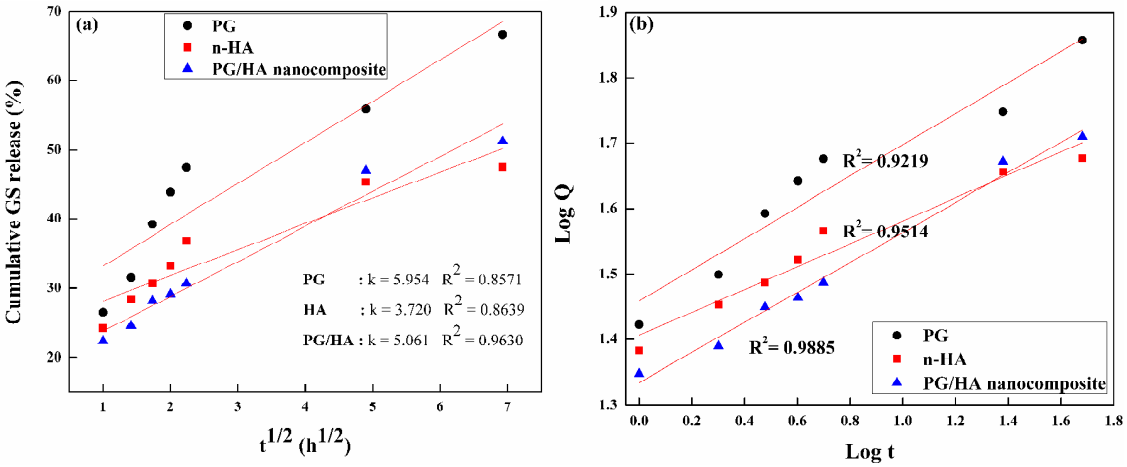

Fig. 9 Plot of (a) Higuchi equation and (b) Ritger-Peppas equation.

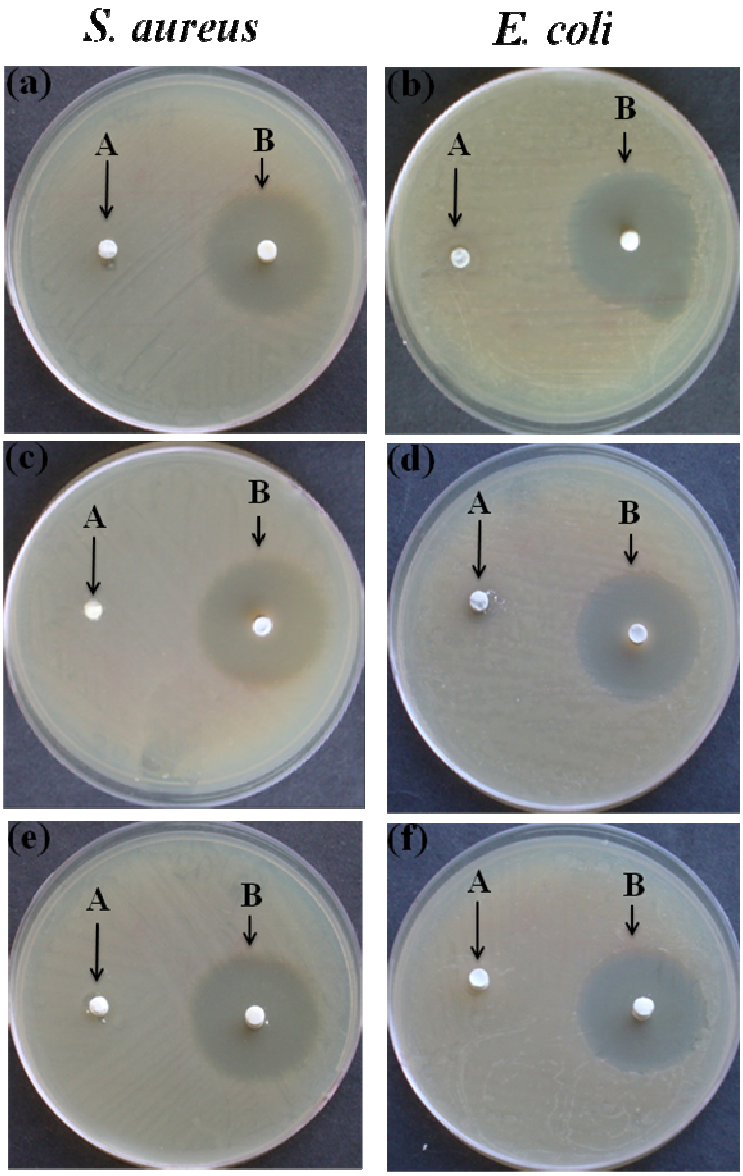

Fig. 10 Antibacterial activity against *S.aureus* and *E. coli,* (a-b) n-HA, (c-d) PG and (e-f) PG/HA nanocomposite. A- Unloaded samples, B- GS loaded samples.

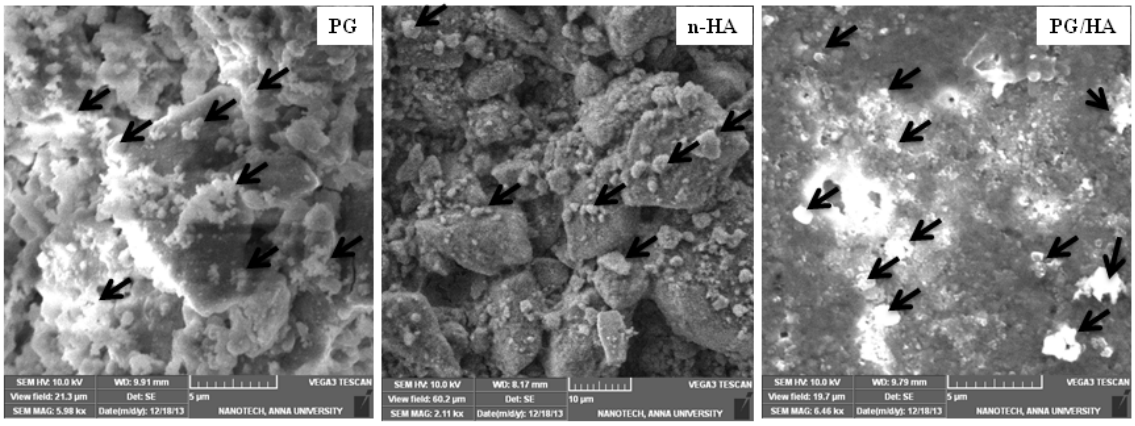

Fig. 11 SEM images of samples after soaking in SBF for 21 days.

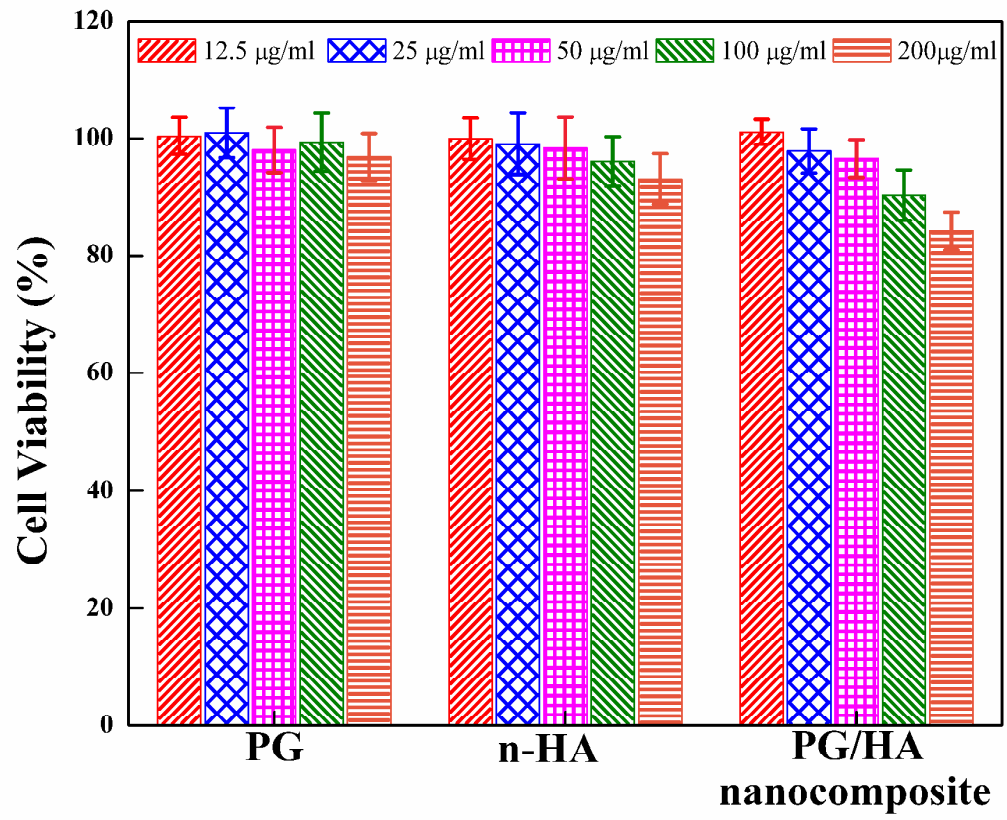

Fig. 12 Cell viability of PG, n-HA and PG/HA nanocomposite with MG63 using MTT assay.

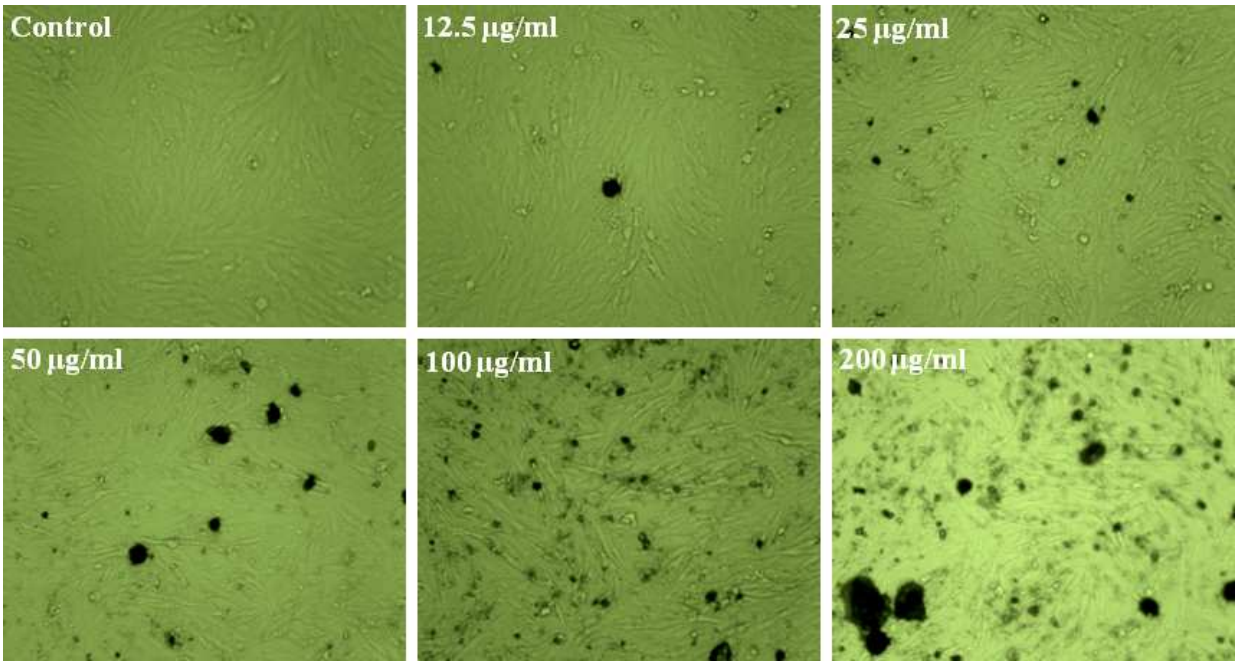

Fig. 13 Optical microscope images of PG/HA nanocomposite with MG63 using MTT assay.

Graphical abstract

Cylindrical shaped gentamicin sulfate (GS) loaded phosphate glass/hydroxyapatite (PG/HA) nanocomposite with sustained release behavior has been developed for osteomyelitis.

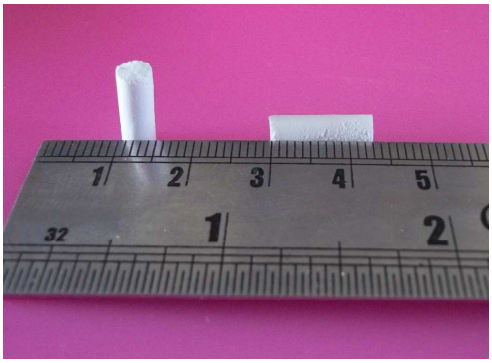

Cylindrical shaped GS loaded PG/HA nanocomposite

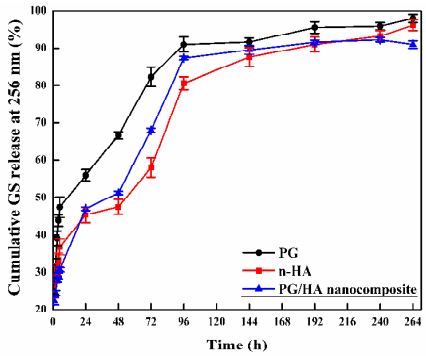

Cumulative GS release from the cylindrical shaped samples